Electronic Supplementary Material (ESI) for Journal of Materials Chemistry A.

Supporting Information

Synthesis of biphenyl bridged dendritic mesoporous organosilica with extremely high adsorption of pyrene

Shevanuja Theivendran[a], Jun Zhang[a], Cheng Tang[b], Mohammad Kalantari[a], Zhengying Gu[a], Yannan Yang[a], Yang Yang[a], Ekaterina Strounina[c], Aijun Du[a], and Chengzhong Yu[a]

[a]Australian Institute for Bioengineering and Nanotechnology, The University of Queensland, Brisbane, Queensland 4072, Australia

[b]School of science and Engineering, Queensland University of Technology, Brisbane, Queensland 4000, Australia

[c]Centre for Advanced Imaging, The University of Queensland, Brisbane, Queensland 4072, Australia

Computational details

The calculations were performed using Vienna Ab Initio Simulation Package (VASP)[1, 2] based on density functional theory (DFT)[3-5] with the Perdew-Burke-Ernzerhof (PBE)[6] generalized gradient approximation (GGA) and projector augmented wave (PAW)[7] pseudopotentials. The kinetic energy cut-off was set to 400 eV. In order to mimic the absorption of pyrene on the phenyl (biphenyl) bridged SiO_2 surface, we used the molecular model in a 30×30×30 cubic unit cell, where the vacuum layers were over 10 Å in all three directions to avoid the interaction between neighboring molecules. The van der Waals correction (DFT+D3) was considered to describe the nonbonding interactions between adsorbents. The surface oxygen atoms of SiO_2 were saturated by hydrogen in our calculations. Additionally, by considering various orientations between pyrene and phenyl (biphenyl) functional group, we obtained the most stable configurations. The absorption energy ($E_{absorption}$) can be calculated through the following equation:

$$\mathbf{E_{absorption} = E_{total} - E_{phenyl\_silica} - E_{pyrene}}$$

Where, the E_{total} and E_{phenyl_silica} represent the total energy of phenyl (biphenyl) bridged organosilicas with and without absorbing pyrene, while E_{pyrene} is the energy of an isolate pyrene molecule.

Pyrene adsorption studies

Pyrene adsorption study was performed based on a previously reported procedure with slight modifications.[8] Pyrene is a hydrophobic organic compound with a solubility of 0.135 mg/L. Therefore, a stock solution of 1mg mL^{-1} in methanol is freshly prepared for all the adsorption studies. In order to mimic the contaminated wastewater model and to ensure the presence of stable homogenous solution, a solution mixture of water: methanol ratio of 7:3 v/v is chosen to tackle with the poor solubility of pyrene in pure water. Pyrene solutions with various concentrations were prepared by dissolving measured quantities of the stock solution in methanol and then ultrapure water was further added to make sure the solution mixture has water to methanol ratio of 7:3 v/v. For the adsorption isotherm studies, 0.25 mg of adsorbent was suspended in 150 mL of aqueous mixture with the initial pyrene concentrations between 0.005 and 0.008 mg/ml. The upper limit of the concentration range (i.e. 0.008 mg/mL) for the adsorption study was chosen by testing the stability of different concentrations with time (Figure S9).The prepared mixtures were shaken for 4 hours at 160 rpm in room temperature. After removal of particles by centrifugation (5000 rpm for 5 min), the equilibrium concentrations of pyrene were calculated by UV-vis absorption spectroscopy at 240 nm (UV-2450, Shimadzu Company) by using a standard curve obtained by a range of pyrene solutions prepared with known concentration at the same water to methanol ratio (Figure S10).

The amount of adsorbed pyrene per unit weight of adsorbent (mg g^{-1}) (Qe) was measured based on the difference in pyrene concentration before and after adsorption using the following equation:

$$Q_e = \frac{(C_0 - C_e) \times V}{W}$$

where C_0 and C_e are the initial and equilibrium concentrations of pyrene (mg mL^{-1}), respectively, V (mL) is the volume of the solution and W (g) is the weight of the adsorbents. To determine the adsorption equilibrium time, the adsorption kinetic experiments were conducted. In a typical procedure, 0.25 mg of adsorbent was suspended in 150 mL of aqueous mixture with pyrene concentration of 0.008 mg/mL. Then the solution was shaken at 160

rpm and room temperature. At each time point, 2 mL of the solution was taken out and the residual concentration of pyrene was measured as previously described.

Table S1: Summary of solid adsorbents and the corresponding adsorption capacities.

Solid adsorbent	$Q_e$max (mg/g)	Year	Reference
Commercial activated carbon	182.84	2007	[9]
Periodic mesoporous organosilica	1.32	2011	[10]
Nature clay	370.3	2011	[11]
Black carbon	10	2011	[12]
Rice husk activated carbon	60	2013	[13]
Silver nanoparticles	0.05	2014	[14]
Mesoporous carbon spheres	77.1	2014	[15]
Cubic mesoporous bridged polysilsesquioxane copolymers	66.1	2014	[16]
Graphene nanosheets	100	2014	[17]
Carbon nanotubes incorporated polyacrylonitrile electrospun nanofibers	0.0025	2015	[18]
Natural sepiolite	8	2017	[19]
Silica aerogel-like material	1.51	2017	[20]
Biochar	44.5	2017	[21]
Pyrene imprinted polymer	0.102	2017	[22]
Clyclodextrin functionalized silica nanoparticles	0.8	2017	[23]
C18 modified mesoporous sorganosilica	757.5	2018	[24]
Sba-15	389.28	2018	[25]
Polystyrene membrane	0.6	2018	[26]
Microplastics	0.16	2018	[27]
Metal organic framework derived carbons	220	2018	[8]

Table S2: Structural parameters of DBMON, DMSN, BOP-1 and S1 after adsorption

Sample ID	***D*** **(nm)**	***d*** **(nm)**	S_{BET} **(m^2/g)**	V_p **(cm^3/g)**
DBMON	195	13.9	729	1.11
DMSN	260	34	482	1.47
BPO-1	-	4.9	651	0.9
S1 after adsorption	357	10.5	12.8	0.059

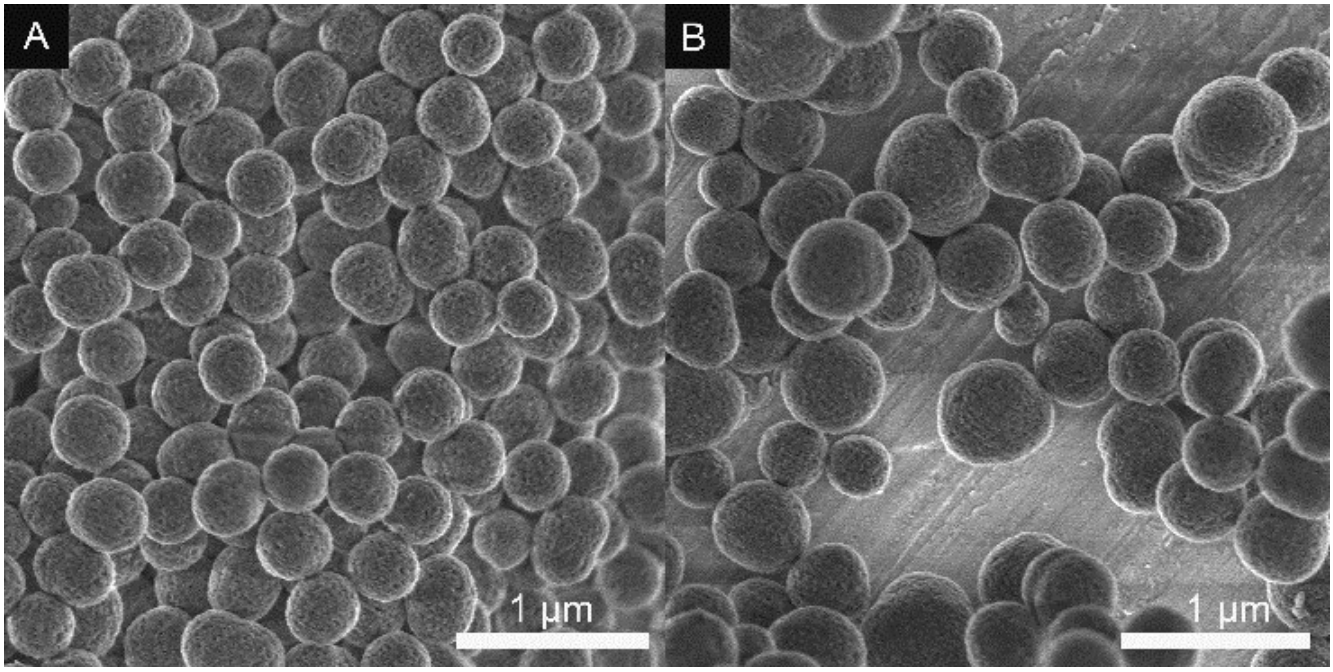

Figure S1: Low magnification SEM images of (A) S1 and (B) S2.

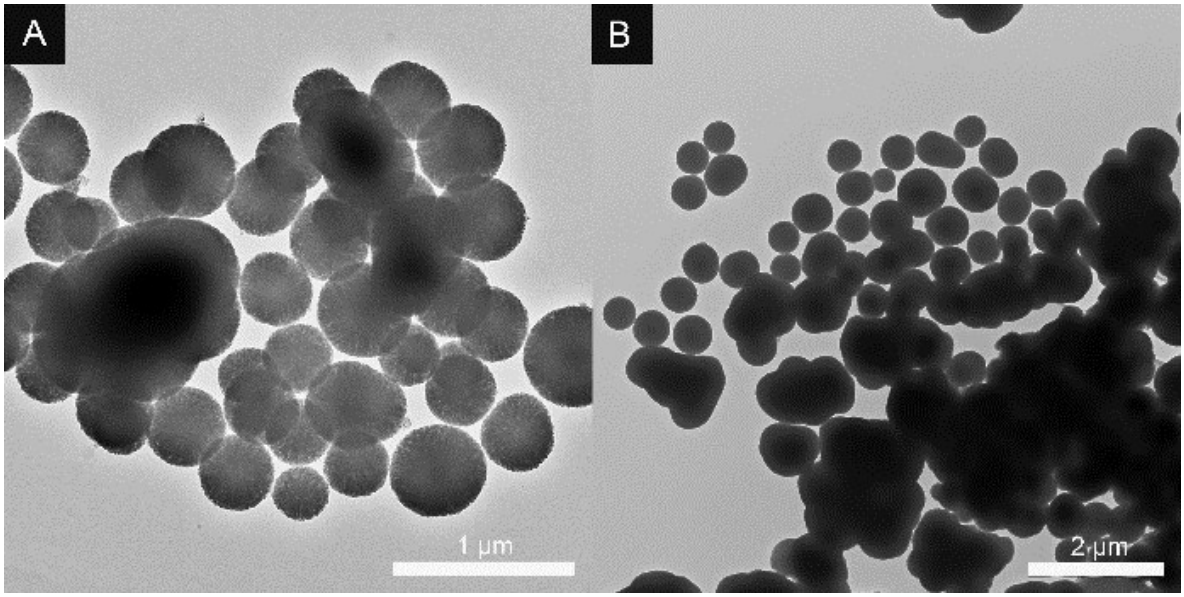

Figure S2: Low magnification TEM images of S2.

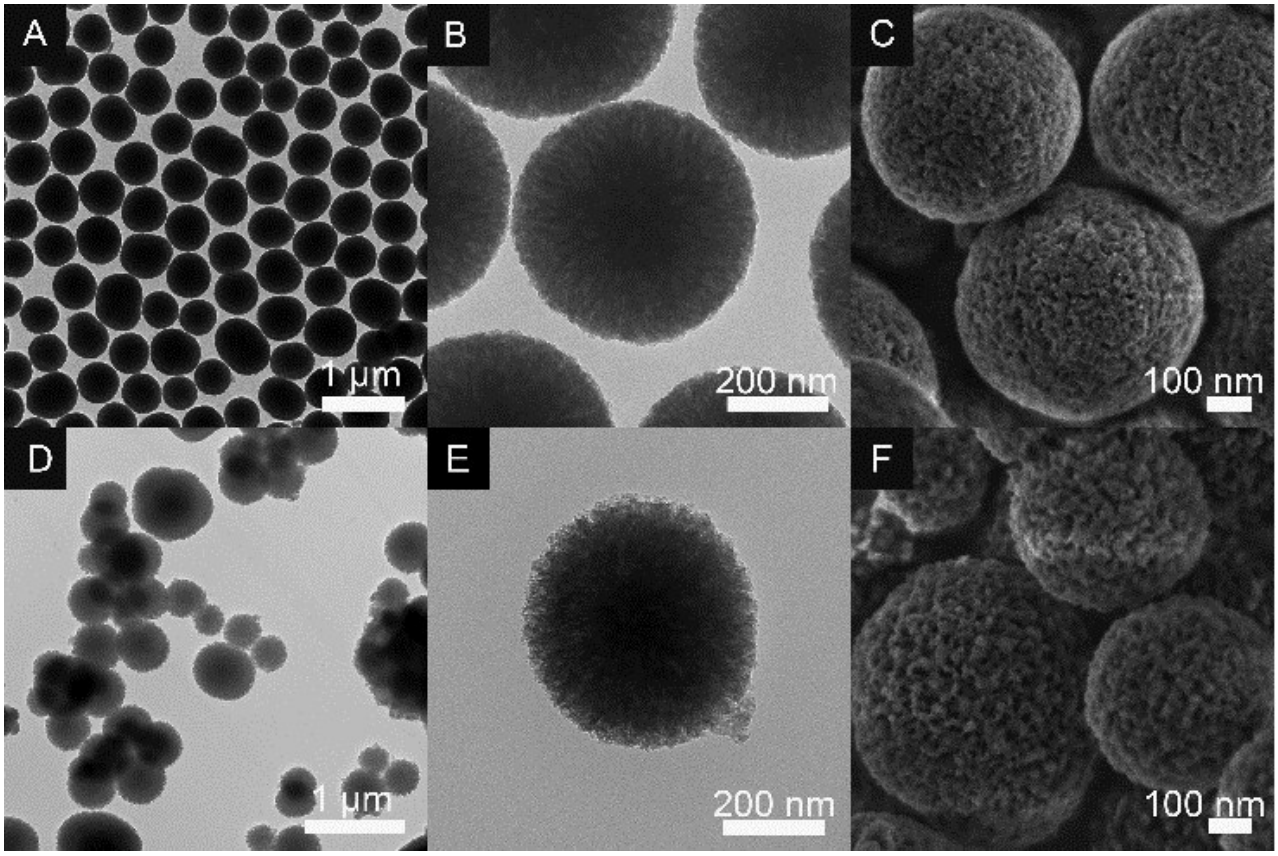

Figure S3: TEM images of (A, B) S3 and (D, E) S4. SEM images of (C) S3 and (F) S4.

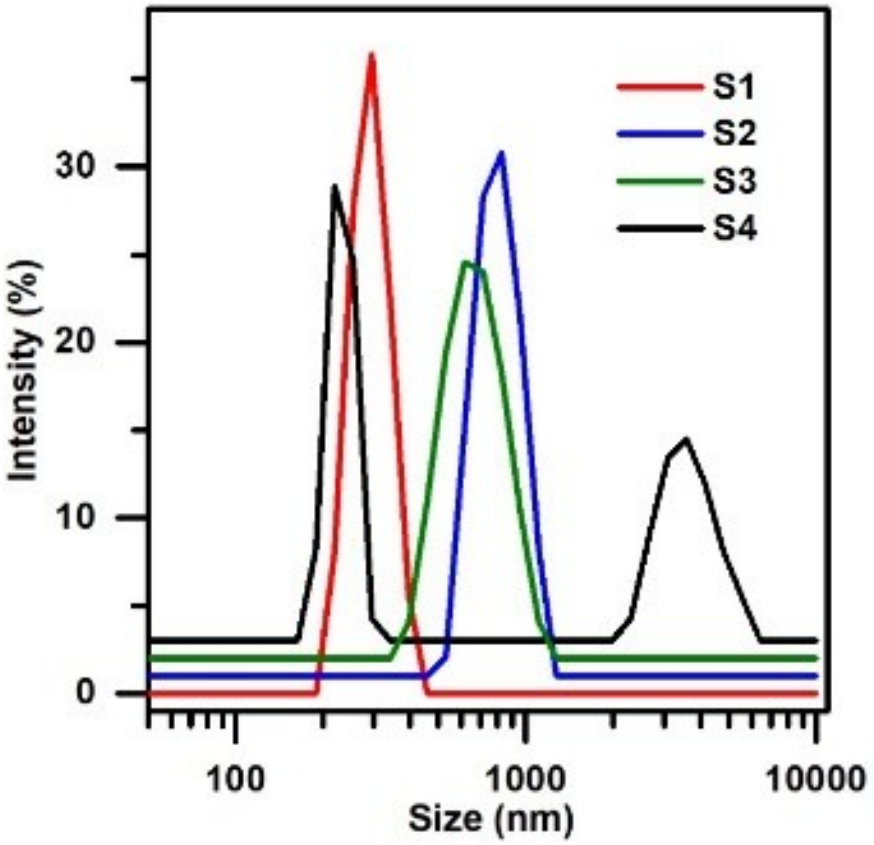

Figure S4: Particle size distribution curves of S1-S4 in ethanol measured by DLS analysis.

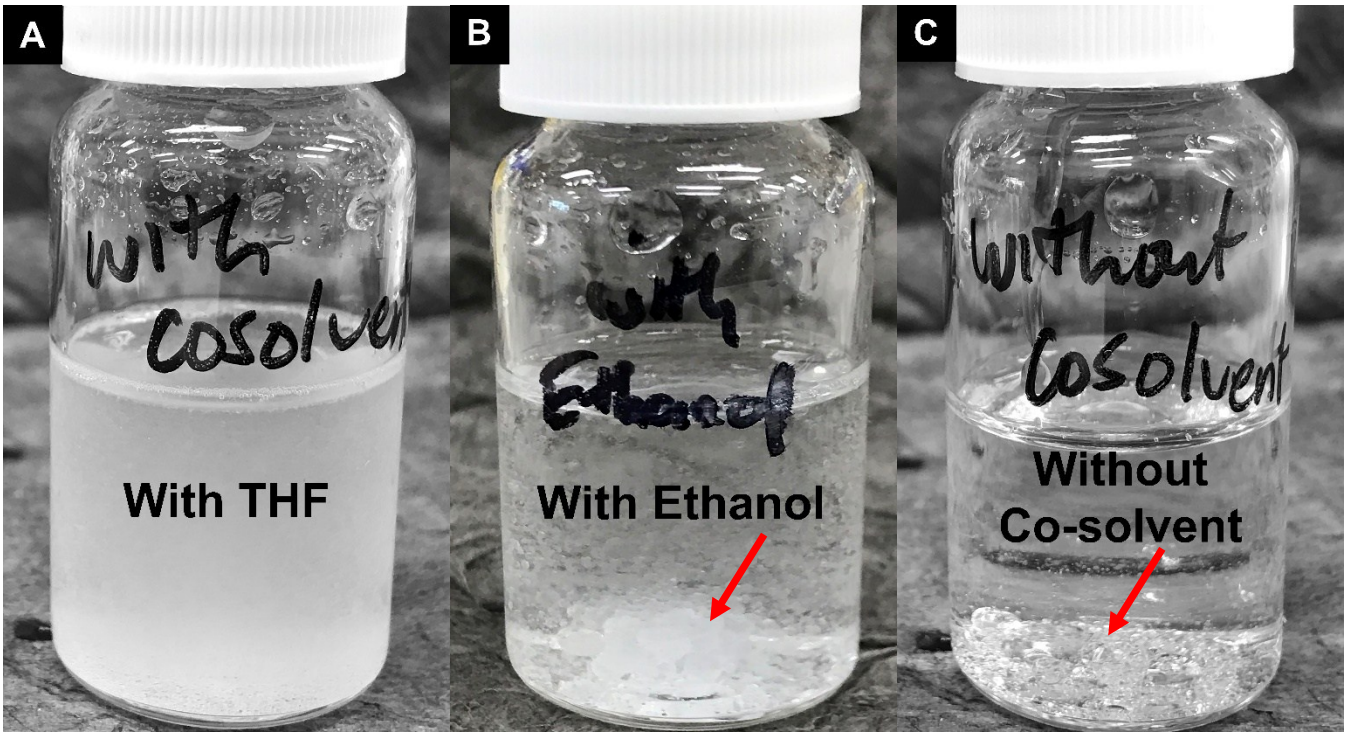

Figure S5: Dispersity of BTEBB oil droplets with different co-solvents (A) THF, (B) ethanol and (C) without any co-solvent in the aqueous media upon quick shaking.

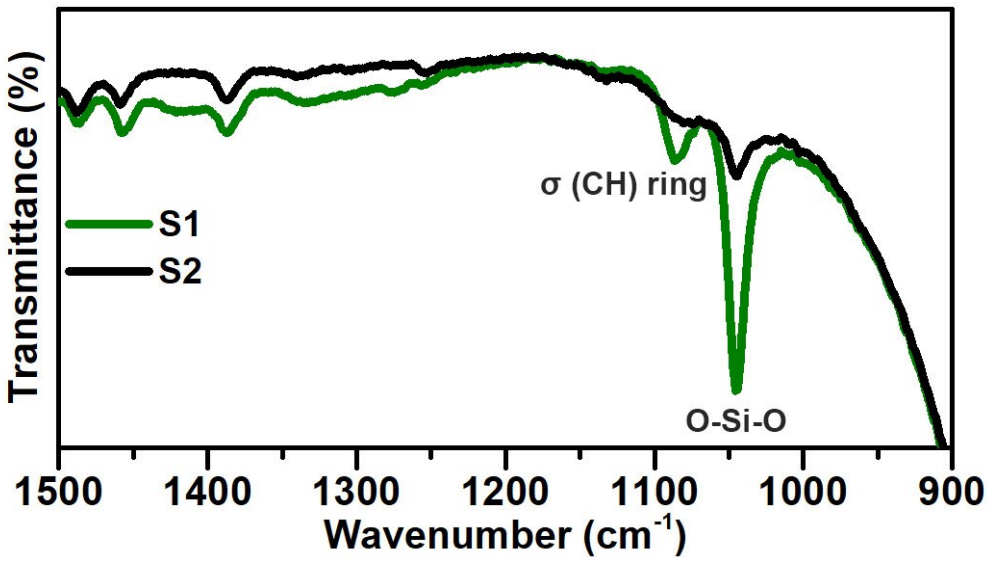

Figure S6: ATR-FTIR spectra of S1 and S2 taken at 12 h time point of the reaction.

Sample window of ATR-FTIR spectrometer was covered with the precipitates obtained from the reaction mixture at 12 h time point. An enhancement in the peak intensity of 1040 cm^{-1} and 1090 cm^{-1}, corresponding to the Si-O-Si bonding and σ (CH) ring of biphenyl group, can be observed for the sample prepared with co-solvent (S1) compared to the one without (S2).

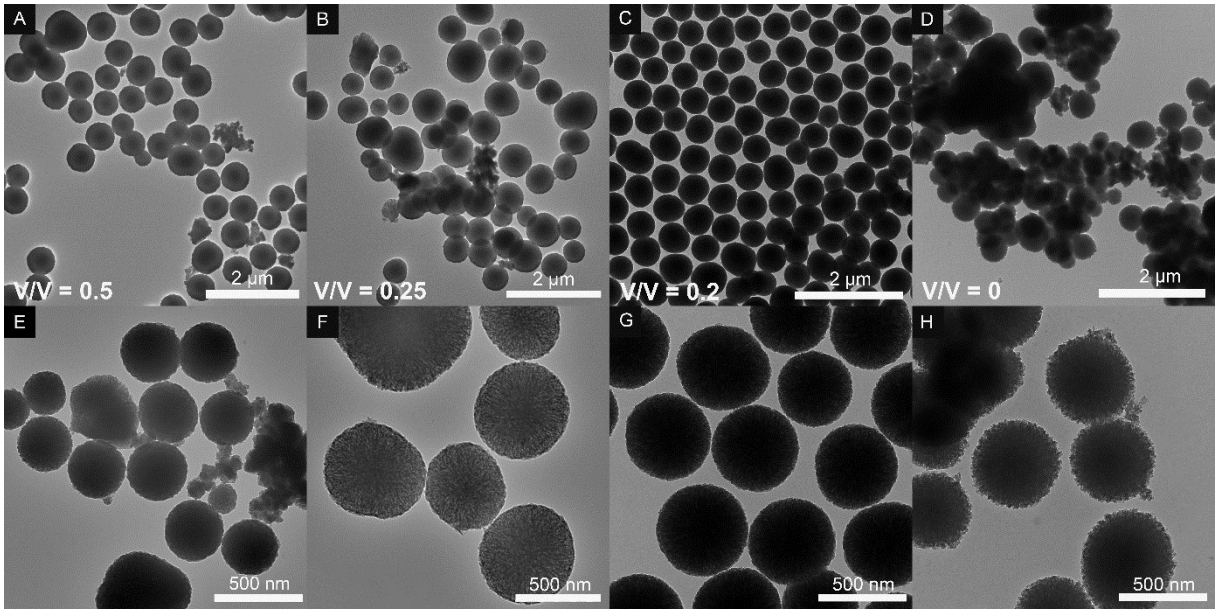

Figure S7: TEM images of BDMON synthesized at 400 RPM and different THF/BTEBB v/v of 0.5 (A,E), 0.25 (B,F), 0.2 (C,G) and 0 (D,H).

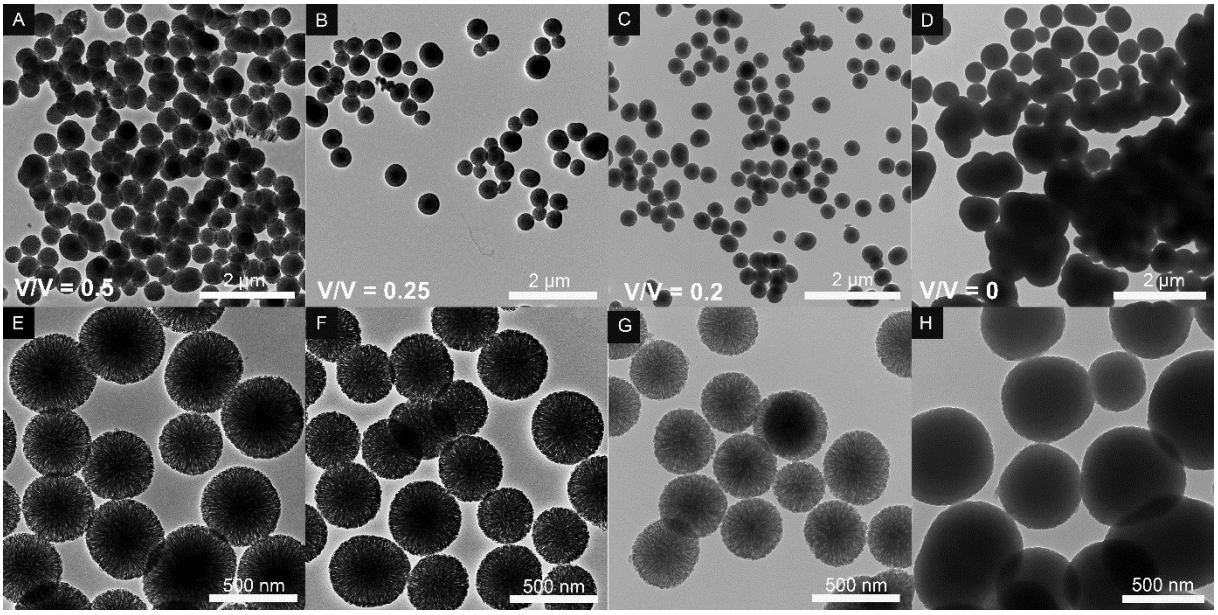

Figure S8: TEM images of BDMON synthesized at 625 RPM and different THF/BTEBB v/v of 0.5 (A,E), 0.25 (B,F), 0.2 (C,G) and 0 (D,H).

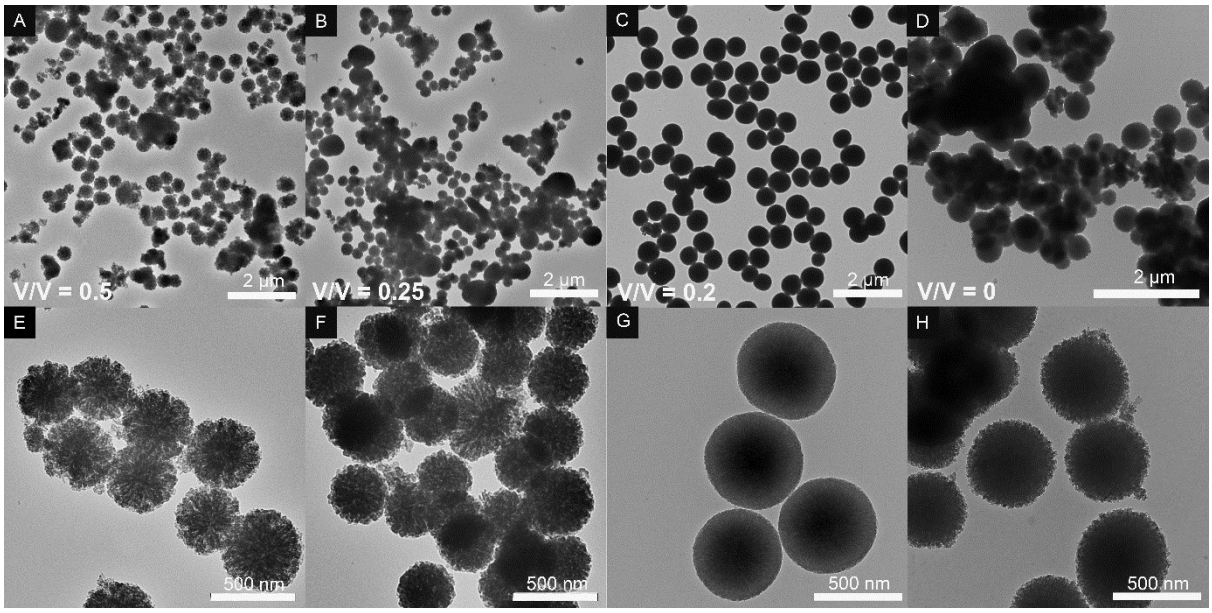

Figure S9: TEM images of BDMON synthesized at 400 RPM and different ethanol/BTEBB v/v of 0.5 (A,E), 0.25 (B,F), 0.2 (C,G) and 0 (D,H).

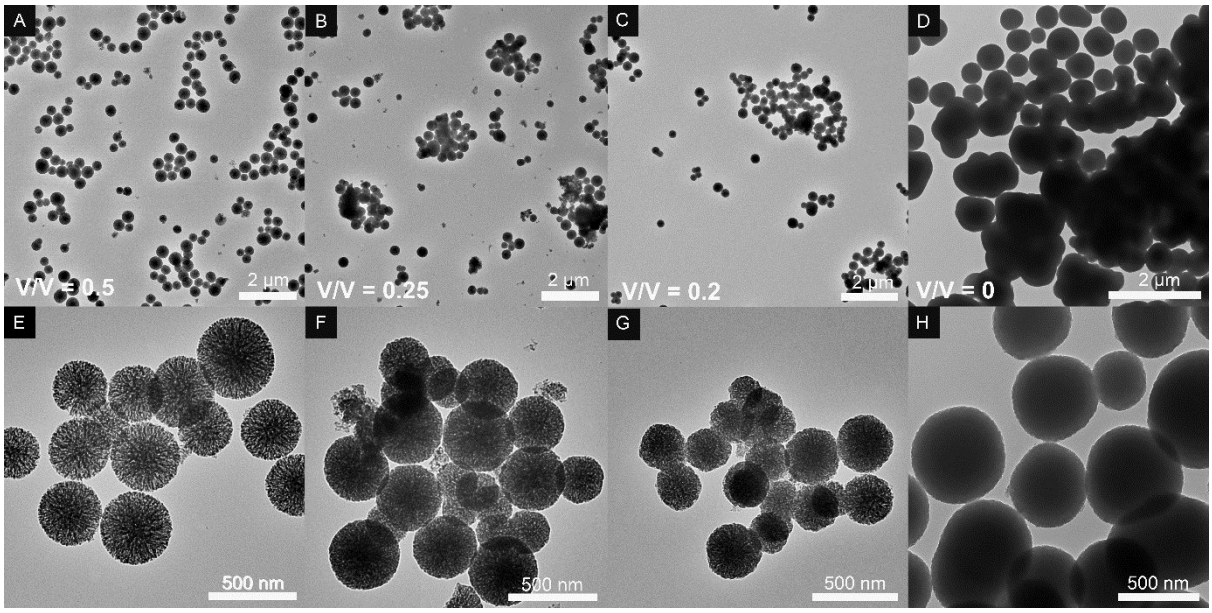

Figure S10: TEM images of BDMON synthesized at 625 RPM and different ethanol/BTEBB v/v of 0.5 (A,E), 0.25 (B,F), 0.2 (C,G) and 0 (D,H).

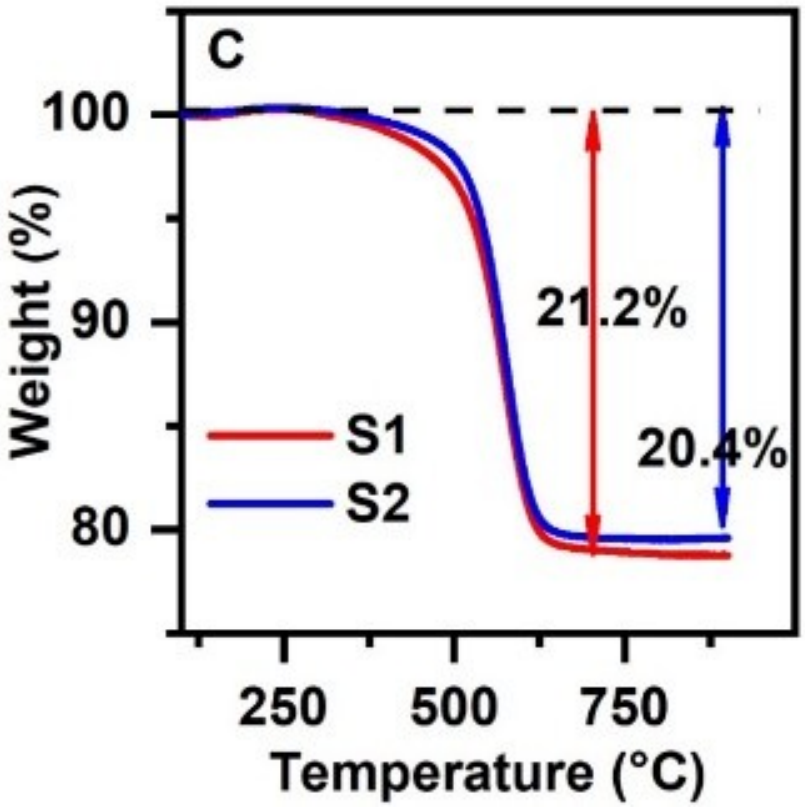

Figure S11: TGA of S1 and S2

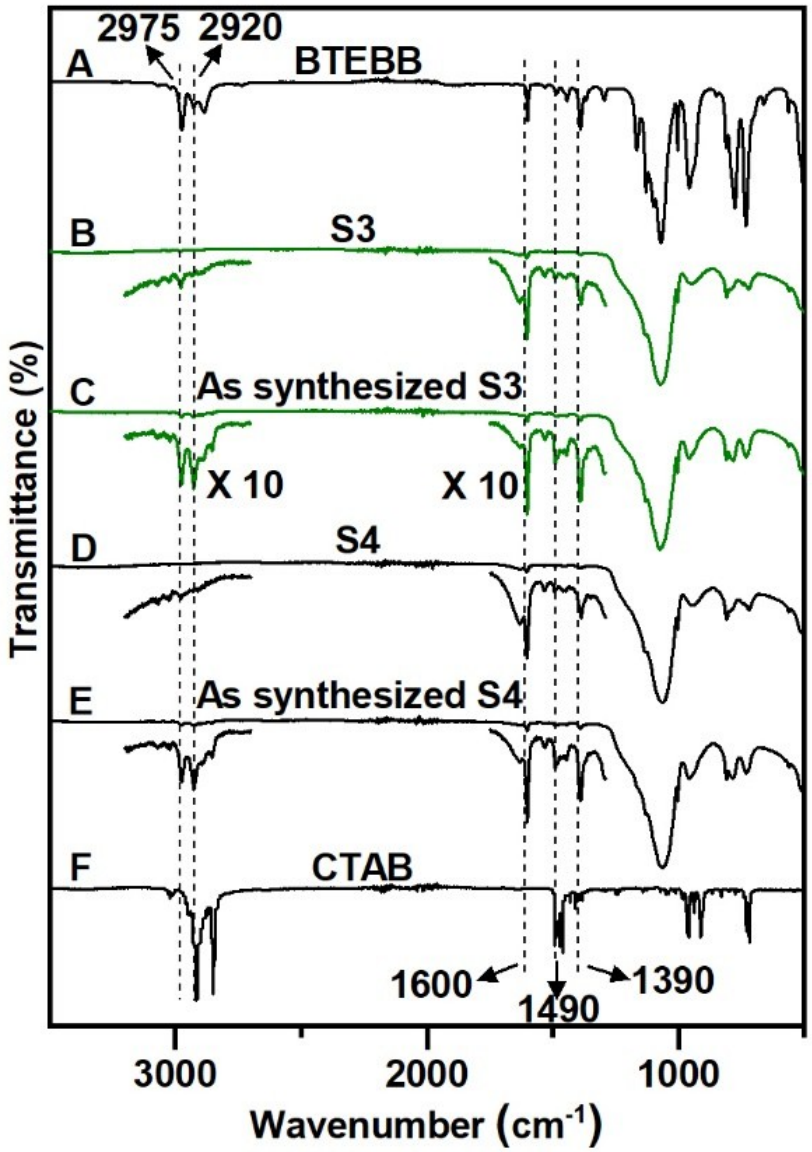

Figure S12: ATR-FTIR spectra of (A) 4,4′-bis(triethoxysilyl)-1,1′-biphenyl, (B) S3, (C) as synthesized S3, (D) S4, (E) as synthesized S4 and (F) CTAB surfactant.

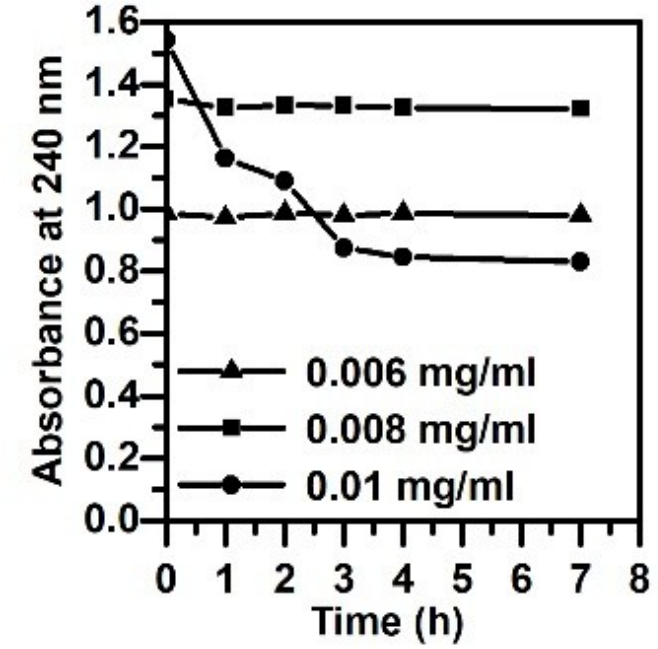

Figure S13: Stability of pyrene at different concentrations (water: methanol ratio of 7:3 v/v) with time.

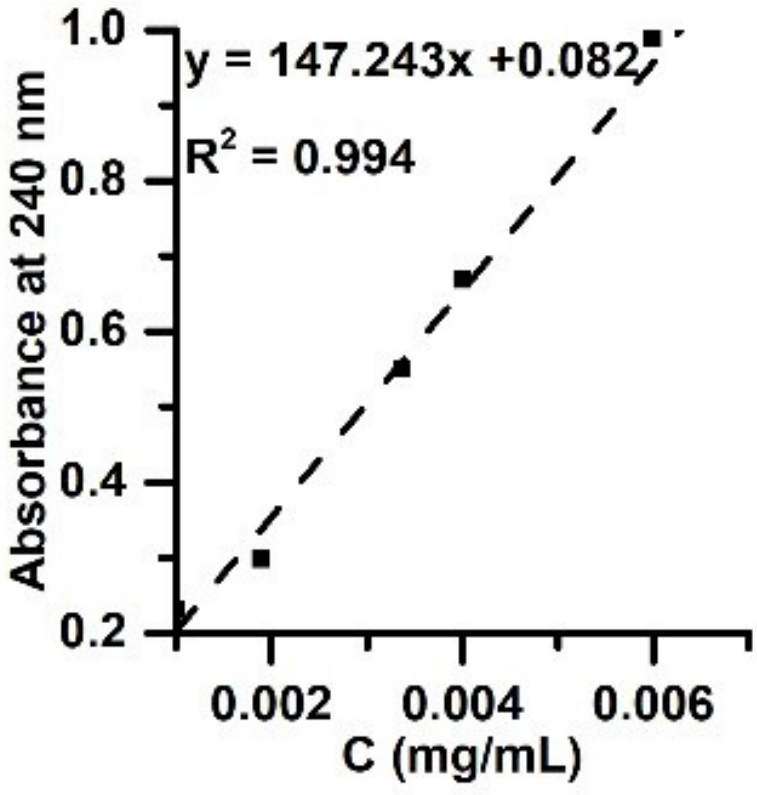

Figure S14: Pyrene standard curve at 240 nm in a water/ methanol = 7/3 v/v solution

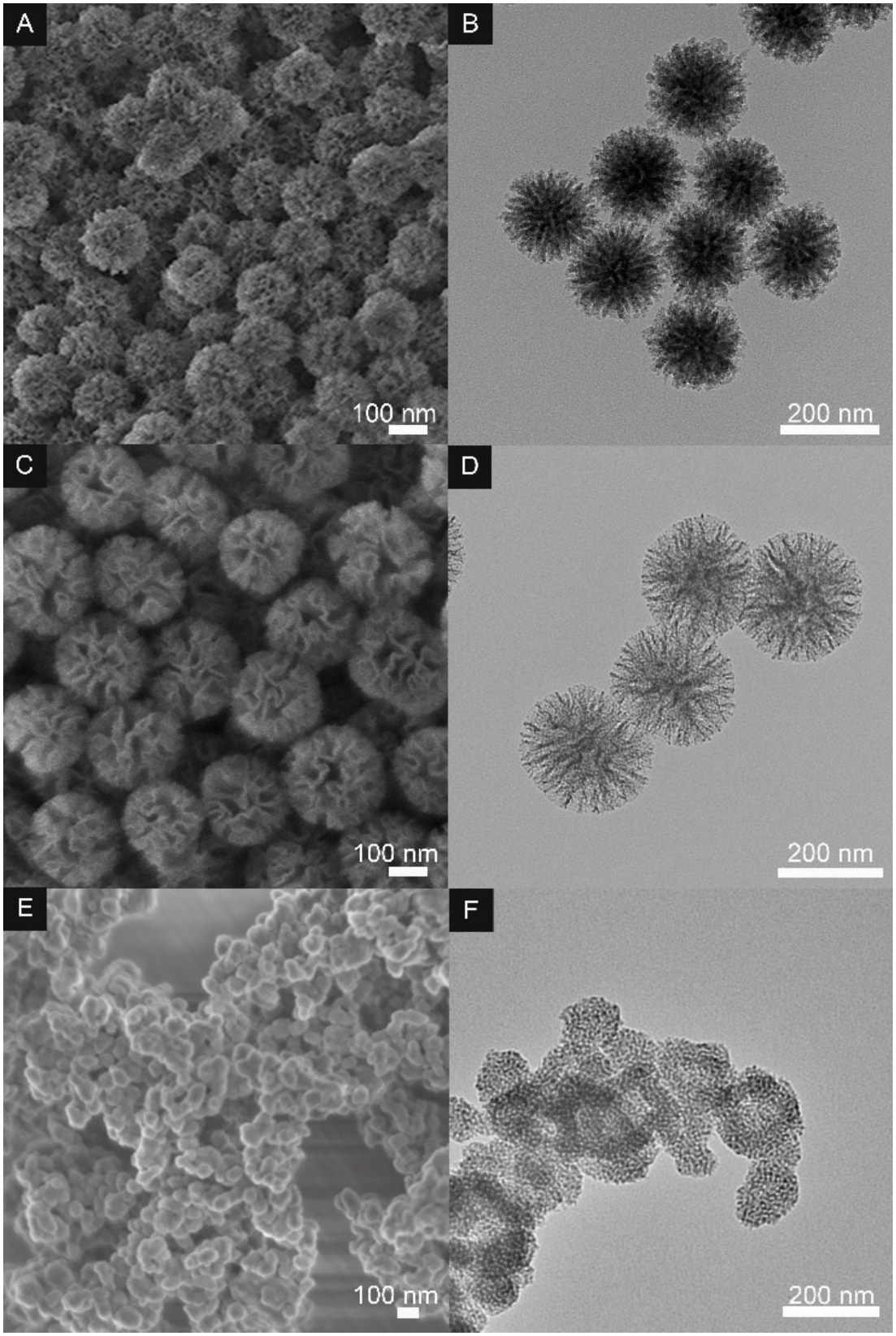

Figure S15: SEM images of (A) DBMON, C) DMSN and (E) BPO-1. TEM images of (B) DBMON, (D) DMSN and (F) BPO-1

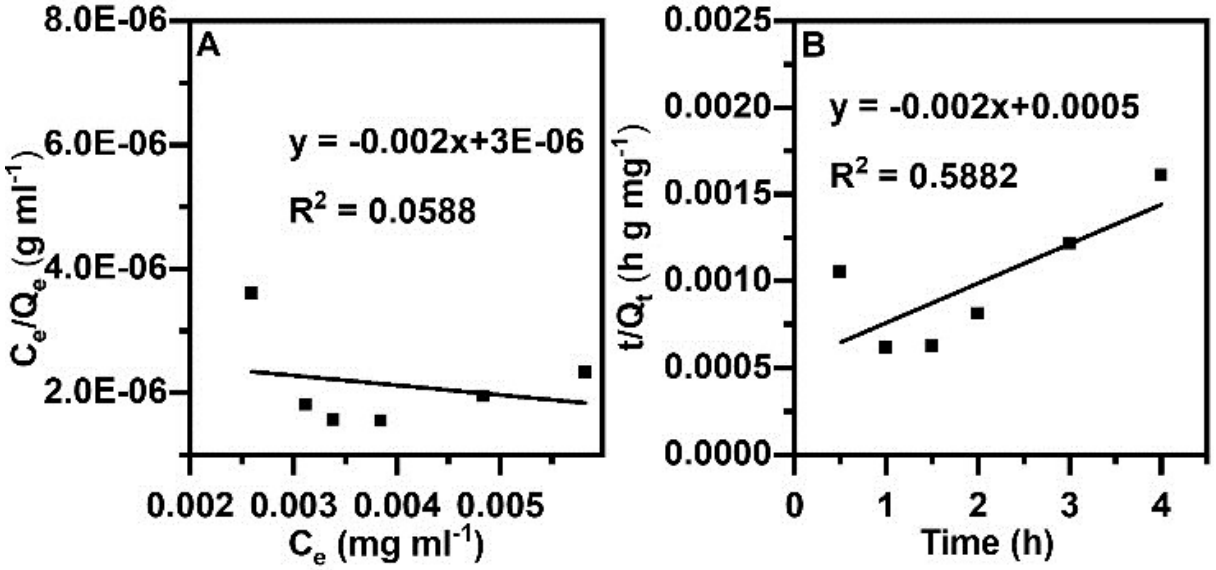

Figure S16: (A) Langmuir fitting and (B) pseudo-second order adsorption kinetics plot for pyrene adsorption on S1.

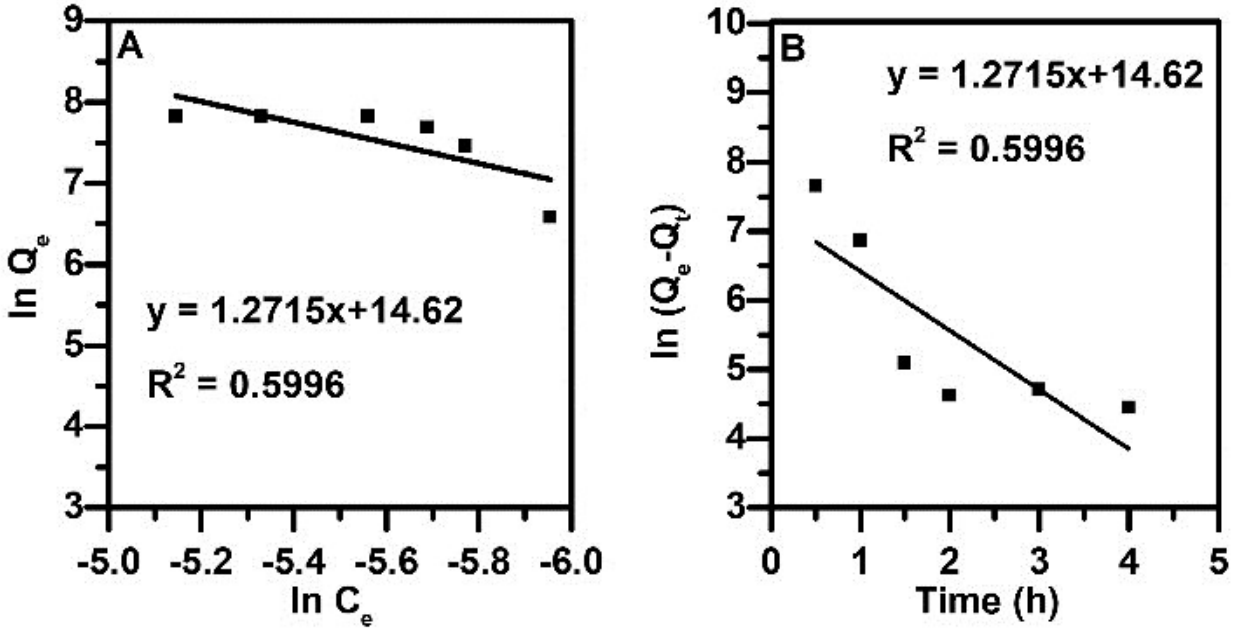

Figure S17: (A) Freundlich fitting (B) pseudo-first order adsorption kinetics plot for pyrene adsorption on S1.

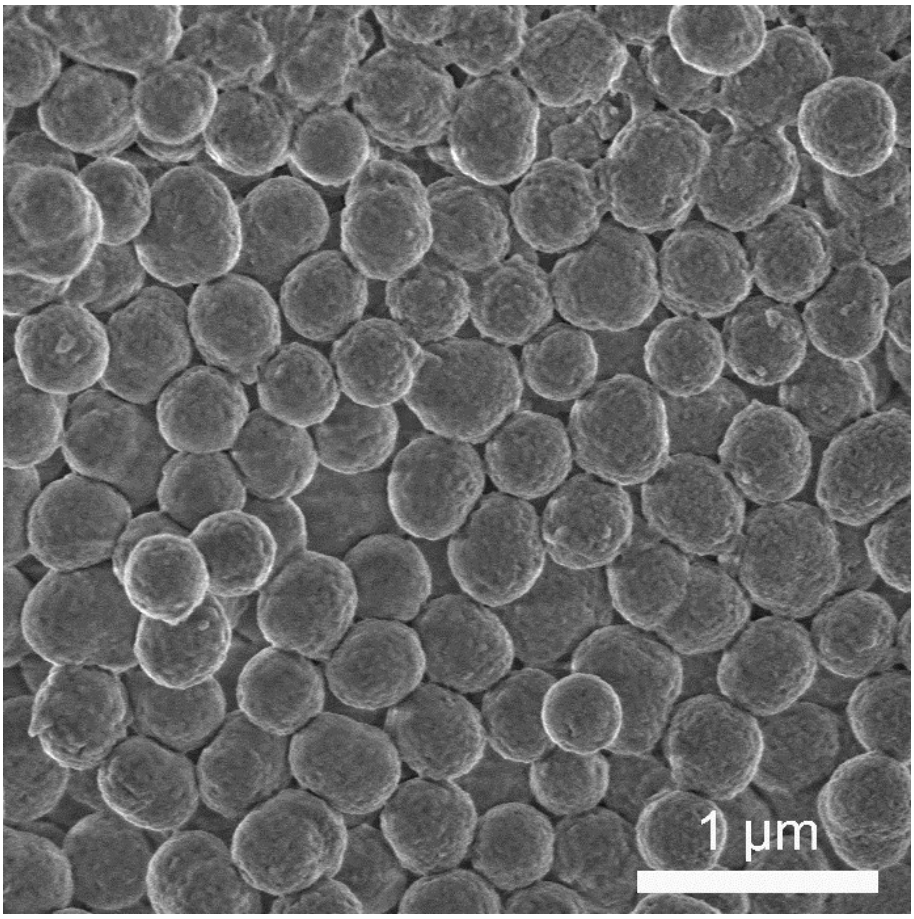

Figure S18: Low magnification of S1 after adsorption of pyrene.

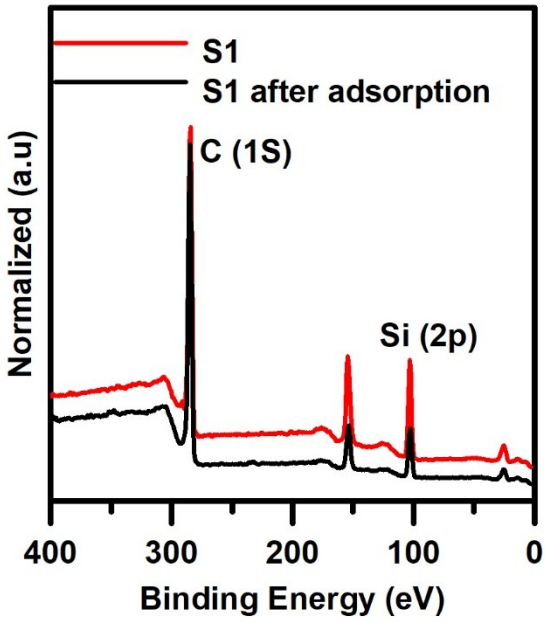

Figure S19: XPS spectra of S1 before and after adsorption of pyrene

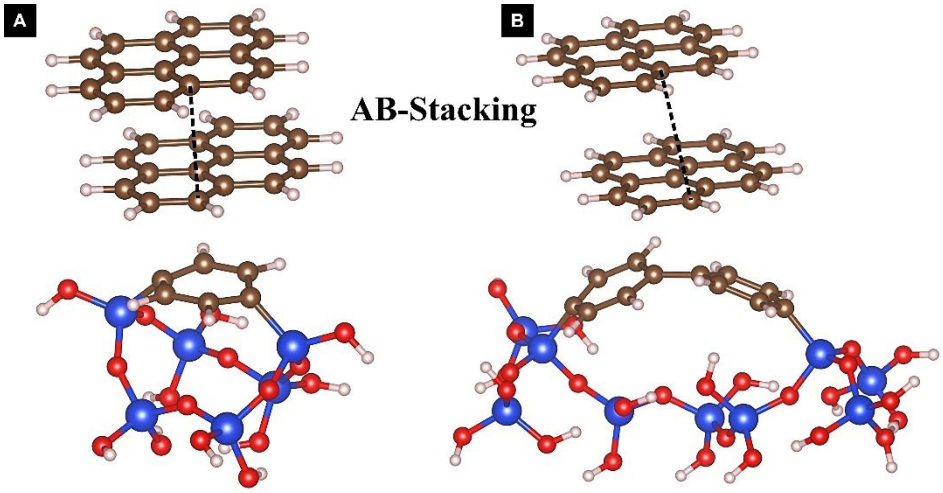

Figure S20: AB stacking configuration for the pyrene-pyrene interaction on (A) phenyl and (B) biphenyl bridged MON

References

1. G. Kresse and J. Furthmüller, *Phys. Rev. B*, 1996, **54**, 11169-11186.
2. G. Kresse and J. Furthmüller, *Comput. Mater. Sci*, 1996, **6**, 15-50.
3. L. J. Sham and M. Schlüter, *Phys. Rev. Lett.*, 1983, **51**, 1888-1891.
4. E. K. U. Gross and W. Kohn, *Phys. Rev. Lett.*, 1985, **55**, 2850-2852.
5. X. Gonze, *Phys. Rev. A*, 1995, **52**, 1096-1114.
6. J. P. Perdew, K. Burke and M. Ernzerhof, *Phys. Rev. Lett*, 1996, **77**, 3865-3868.
7. G. Kresse and D. Joubert, *Phys. Rev. B*, 1999, **59**, 1758-1775.
8. B. N. Bhadra, J. Y. Song, S.-K. Lee, Y. K. Hwang and S. H. Jhung, *J Hazard Mater*, 2018, **344**, 1069-1077.
9. A. M. Dowaidar, M. S. El-Shahawi and I. Ashour, *Sep. Sci. Technol.*, 2007, **42**, 3609-3622.
10. C. B. Vidal, A. L. Barros, C. P. Moura, A. C. A. de Lima, F. S. Dias, L. C. G. Vasconcellos, P. B. A. Fechine and R. F. Nascimento, *J. Colloid Interface Sci.*, 2011, **357**, 466-473.
11. J. J. Liu, X. C. Wang and B. Fan, *Bioresour Technol*, 2011, **102**, 5305-5311.
12. W. Zhang, L. Wang and H. Sun, *Chemosphere*, 2011, **85**, 1306-1311.
13. A. A. M. D. S.M. Yakout, and S.A. El-Reefy, *Asian J. Chem.*, 2013, **25**, 10037-10042.
14. M. Abbasi, F. Saeed and U. Rafique, *IOP Conference Series: Mater. Sci. Eng*, 2014, **60**, 012061.
15. W.-j. Liu, Y.-x. Liu, X.-y. Yan, G.-p. Yong, Y.-p. Xu and S.-m. Liu, *J. Mater. Chem. A*, 2014, **2**, 9600-9606.
16. D.-R. Lin, L.-J. Hu, B.-S. Xing, H. You and D. A. Loy, *Materials (Basel, Switzerland)*, 2015, **8**, 5806-5817.
17. J. Wang, Z. Chen and B. Chen, *Environ. Sci. Technol.*, 2014, **48**, 4817-4825.
18. A. H. Jadhav, X. T. Mai, F. A. Ofori and H. Kim, *Chem Eng J.,* 2015, **259**, 348-356.
19. E. Sabah and S. Ouki, *Environ Sci Pollut Res*, 2017, **24**, 21680-21692.
20. C. M. C. Filho, T. Matias, L. Durães and A. J. M. Valente, *Colloids Surf A Physicochem Eng Asp.*, 2017, **520**, 550-560.
21. W. Guo, Y. Ai, B. Men and S. Wang, *Int. J. Environ. Sci. Technol.*, 2017, **14**, 1889-1896.
22. R. W. Kibechu, S. Sampath, B. B. Mamba and T. A. M. Msagati, *J. Appl. Polym. Sci.*, 2017, **134**, 45300.
23. F. Topuz and T. Uyar, *J. Colloid Interface Sci.*, 2017, **497**, 233-241.
24. M. Kalantari, Y. Liu, E. Strounina, Y. Yang, H. Song and C. Yu, *J. Mater. Chem. A*, 2018, **6**, 17579-17586.
25. P. Yuan, X. Li, W. Wang, H. Liu, Y. Yan, H. Yang, Y. Yue and X. Bao, *Langmuir*, 2018, **34**, 15708-15718.
26. Y. Li, H. Pu, J. Cheng, J. Du, H. Pan and Z. Chang, *J. Appl. Polym. Sci.*, 2018, **135**, 45917.
27. W. Wang and J. Wang, *Chemosphere*, 2018, **193**, 567-573.